Bull Volcanol (2006) 68: 480–490
DOI 10.1007/s00445-005-0023-8

RESEARCH ARTICLE

Mario C. Ruiz · Jonathan M. Lees · Jeffrey B. Johnson

Source constraints of Tungurahua volcano explosion events

Received: 24 January 2005 / Accepted: 29 August 2005 / Published online: 16 December 2005

Abstract The most recent eruptive cycle of Tungurahua volcano began in May 2004, and reached its highest level of activity in July 2004. This activity cycle is the last one of a series of four cycles that followed the reawakening and major eruption of Tungurahua in 1999. Between June 30 and August 12, 2004, three temporary seismic and infrasonic stations were installed on the flanks of the volcano and recorded over 2,000 degassing events. The events are classified by waveform character and include: explosion events (the vast majority, spanning three orders of pressure amplitudes at 3.5 km from the vent, 0.1–180 Pa), jetting events, and sequences of repetitive infrasonic pulses, called chugging events. Travel-time analysis of seismic first arrivals and infrasonic waves indicates that explosions start with a seismic event at a shallow depth (<200 m), followed ~1 s later by an out-flux of gas, ash and solid material through the vent. Cluster analysis of infrasonic signals from explosion events was used to isolate four groups of similar waveforms without apparent correlation to event size, location, or time. The clustering is thus associated with source mechanism and probably spatial distribution. Explosion clusters do not exhibit temporal dependence.

Keywords Volcanic degassing · Volcanic explosions · Cluster analysis · Tungurahua

Editorial responsibility: M. Ripepe

M. C. Ruiz (✉) · J. M. Lees
Department of Geological Sciences, University of North Carolina,
Mitchell Hall - Campus Box #3315, Chapel Hill, NC 27599-3315, USA
e-mail: mruiz@email.unc.edu
Tel.: +919-966-4519
Fax: +919-843-5472

M. C. Ruiz
Instituto Geofisico, Escuela Politecnica Nacional,
Quito, Ecuador

J. B. Johnson
Climate Change Research Center, University of New Hampshire,
Durham, New Hampshire, USA

Introduction

Tungurahua volcano (1.45°S, 78.43°W) is one of the most active volcanoes of the Ecuadorean Andes. Its current volcanic cone has steep flanks (30–35°) and an open crater in the upper part of its northwestern flank. This cone is built over two ancient edifices that were destroyed by large debris avalanches (Hall et al. 1999). Since colonial times (1534), Tungurahua has produced five eruptive periods: 1640–1641, 1773–1777, 1886–1888, 1916–1918, and 1999–present (Egred 2004), totaling seven major emissions of lava, pyroclastic flows and fallout tephra with silica content ranging from 56.8 to 65.5% (Hall et al. 1999). The current crater has been the emission point for all these eruptions.

Appearance of volcanic tremor in 1993 preceded the last eruptive period (Ruiz et al. 1999), whose first explosion occurred on October 5 1999, and was followed by a significant activity in November–December 1999 (Molina 2001). On October 17th, the alert level at Tungurahua volcano was raised to Orange, leading to an evacuation of over 26,000 people from Baños, a town 8 km from the summit, as well as other villages surrounding the volcano area (Tobin and Whiteford 2002). Activity in November and December 1999 was dominated by ash-and-tephra falls on the west flank and mushroom-shaped columns sometimes extending higher than 7 km (Instituto Geofisico 2001). During this time period, however, no pyroclastic flows occurred. After November, volcanic activity decreased and the majority of evacuees returned to Baños on January 5, 2000 (Instituto Geofisico 2001).

Since the sizable eruptive activity in late 1999 ended, Tungurahua exhibited four eruptive cycles (Fig. 1). The most recent eruptive cycle started in late May 2004, reached its climax in July, and waned in the early part of 2005. Diverse measurements carried out by the Geophysical Institute of the National Polytechnic School of Ecuador (IG-EPN) confirmed that Tungurahua reached a moderate activity level during the most recent period (May–December 2004) with frequent ash columns of altitudes no higher than 3 km above the crater. COSPEC measurements carried out by IG-EPN (Instituto Geofisico-OVT, 2004) indicated SO_2

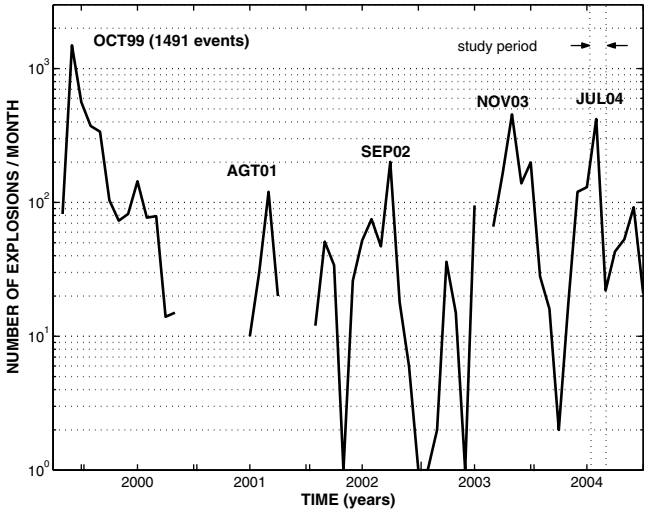

Fig. 1 Monthly number of explosions recorded by the seismic network of Instituto Geofisico in log scale is given by the *dark line*. Peaks of activity are labeled with a month-year code. 2004 summer deployment is marked by *arrows*. Data compiled from Instituto Geofisico data base

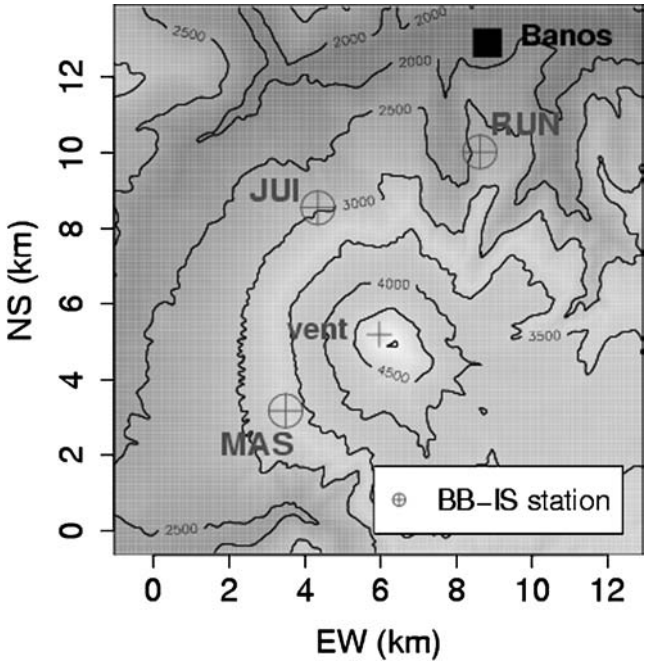

Fig. 2 Location of broad-band seismic-infrasonic stations (BB-IS) deployed on June–August 2004 on SW (MAS), NW (JUI) and NE (RUN) flanks of Tungurahua volcano. Vertical and horizontal axes are in kilometers

concentrations of 65 t/h (07/08/04) and 81 t/h (07/28/04), showing that Tungurahua had slightly higher degassing levels than the 2003–2004 background (43.1±27.9 t/h). Despite this activity level, approximately 25,000 people reside in high-risk areas such as Baños and small villages and farms on the volcanic flanks.

In October 1999, a temporary infrasonic microphone was deployed on a ridge just in front of the northwestern flank. During a 4-day operation, this instrument recorded series of explosion pulses and an almost continuous jetting signal (Johnson et al. 2003). In addition, a low-frequency microphone installed at the headquarters of the Tungurahua Volcano Observatory (∼13 km from the vent) recorded 14 infrasonic explosion signals from August 11 through August 31, 2000. All the infrasonic signals began with a single compression-rarefaction pulse in a low frequency band (0.5–2.1 Hz). Explosion signals have been further observed with ground-coupled waves at seismic stations, especially at station PATA (4.6 km from the vent). The time difference between P waves and infrasonic ground-coupled waves ranges from 11 to 16 s at PATA with a mean of 13.3 s (Ruiz et al. 2001). In this paper, we describe a temporary deployment of three seismic and infrasonic stations installed in the summer of 2004 to monitor explosion activity and further constrain source locations of eruptions at Tungurahua.

Experiment description

In late June 2004, two stations (RUN and MAS) with collocated seismic and infrasonic sensors were deployed on the NE and SW flanks. Another station (JUI) was deployed on the NW flank on July 19, 2004. These instruments were located at horizontal distances between 3.20 and 5.51 km from the active vent (Fig. 2; Table 1). Power failures due to ash falls, wind, and heavy rains occasionally affected the instrument operation. However, more than 2,300 seismic events were recorded between June 29 and August 12, 2004, and most of these (2,142) were related to the volcanic activity. Others correspond to tectonic activity, especially the earthquakes of the Pisayambo seismogenic zone, and the main shock and aftershock sequence of a local 4.2 tectonic earthquake (July 30, 2004).

Table 1 Description and location of instrumentation

Station	Sensors	Gains	Response	Latitude S	Longitude W	Altitude	Total distance
MAS	CMG40T	802 v/m/s	30 s–50 Hz	−1.4836°	−78.4684°	3,310 m	3,516 m
	LD 2570	48.4 mv/Pa	>0.2 Hz				
JUI	CMG40T	800 v/m/s	30 s–50 Hz	−1.4353°	−78.4607°	2,965 m	4,168 m
	LD 2570	48.4 mv/Pa	>0.2 Hz				
RUN	CMG3T	1496 v/m/s	114 s–50 Hz	−1.4221°	−78.4223°	2,700 m	5,889 m
	LD 2570	48.4 mv/Pa	>0.2 Hz				

Table 2 Distinctive characteristics of degassing signals at Tungurahua volcano

Signal type	EX	RO	CH
Seismic signal	First arrival on vertical component is emergent with compressive polarity in all azimuths. Waveform envelope has spindle shape. Ground-coupled acoustic signal is noticeable	Emergent: waveform envelope has spindle shape. No ground coupled acoustic signals are apparent. Small amplitudes	Emergent: no explosion event as a trigger. Waveforms have tremor-like envelopes. No ground coupled acoustic signal is apparent. Small amplitudes
Infrasonic signal	Clear compressive pulse followed by rarefaction and small amplitude coda. Frequency 1–3 Hz. Some events are followed by a high-frequency rumbling (up to 62 Hz). Large range of amplitudes (up to 180 Pa)	Emergent first arrival waves are followed by a chaotic wave train with larger amplitudes. This starts with a very small blast in a few cases. Frequencies 1–10 Hz	Sequence of compressive pulses with time intervals between 0.5–1.0 s. No clear gliding is seen

Description of degassing signals

Degassing events, characterized by the presence of concurrent seismic and acoustic signals, comprise 95% of volcanic seismic signals recorded at Tungurahua during the 2004 deployment. Degassing signals are classified as: explosions (EX), jetting signals (roars, RO), and chugging events (CH), based on waveform characteristics summarized in Table 2. Local seismic signals without an acoustic (infrasonic) component have been classified as: Long Period (LP), Hybrid (HB), Volcano-tectonic (VT), and Tremor (TR) (Power et al. 1994). Figure 3 shows the distribution of these categories.

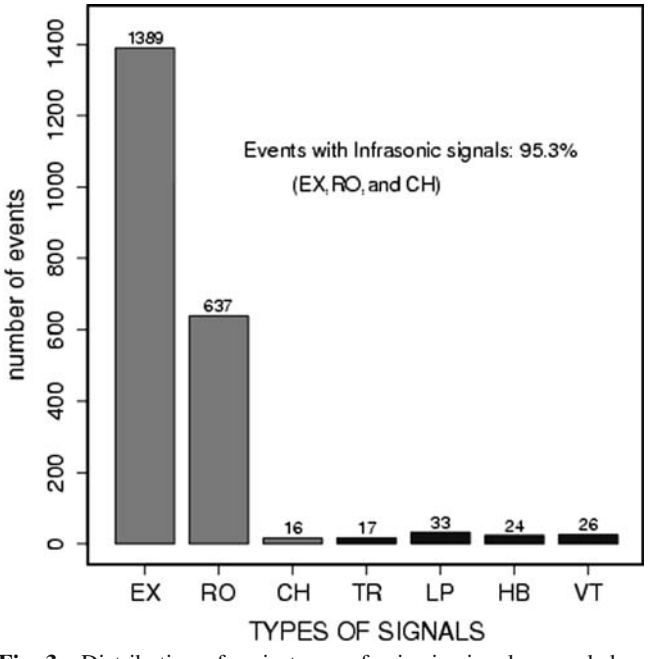

Fig. 3 Distribution of main types of seismic signals recorded on Tungurahua. Explosions (*EX*), jetting (or roars *RO*), and chugging (*CH*) events have acoustic signals. These events are related to degassing processes, and account for more than 95% of total volcanic signals. Tremor (*TR*), Long-Period (*LP*), Hybrid (*HY*), and Volcanic-Tectonic (*VT*) events do not have an acoustic component

Explosions

At all stations, infrasonic records of EX events (Fig. 4A) have impulsive compression onsets, followed by rarefaction pulses, and a short duration coda with an exponential decaying envelope. These signals contain more energy in the 1–3 Hz band without a very long period component, and are similar to explosion signals recorded on Sakurajima (Garcés et al. 1999), Sangay (Johnson and Lees 2000), Karymsky (Johnson and Lees 2000), Arenal (Hagerty et al. 2000), and Fuego (Johnson et al. 2004). Amplitudes of EX signals span three orders of magnitude from 0.1 to 180 Pa (July 21, 03h32 GMT, the largest signal recorded on MAS station). Often initial EX infrasound is followed by a tremor-like signal (Fig. 4B) with irregular envelope and wide frequency content (up to the signal's Nyquist frequency of 62.5 Hz). Time lapses between the impulsive explosion blast and the tremor-like signal range from 5 to 100 s. Several of these high frequency signals have larger pressure amplitudes than the initial blast.

Seismic signals of explosion events (Fig. 4C and D) are characterized by an emergent compressive onset on vertical components (T_{p1}), followed by a secondary compressive phase (T_{p2}). Some seismic waveforms have very clear ground-coupled airwaves with high frequency content.

Jetting signals

Waveforms of jetting signals (roars) are characterized by emergent initial arrivals with long duration codas both in seismic and infrasonic records (Fig. 5A and C). No clear blasts are associated with the initiation of these signals. Acoustic records of some eruptions from Stromboli (Woulff and McGetchin 1976) have an appearance similar to the one observed in RO events including (1) emergent onset, (2) coda punctuated by distinct peaks, and, (3) a gradual decay to background. Dominant amplitudes span the 1–4 Hz band with no significant energy above 10 Hz. In a few cases, however, jetting events seem to be generated by overlapping series of smaller explosions; but in general, no single blast signals are recognized.

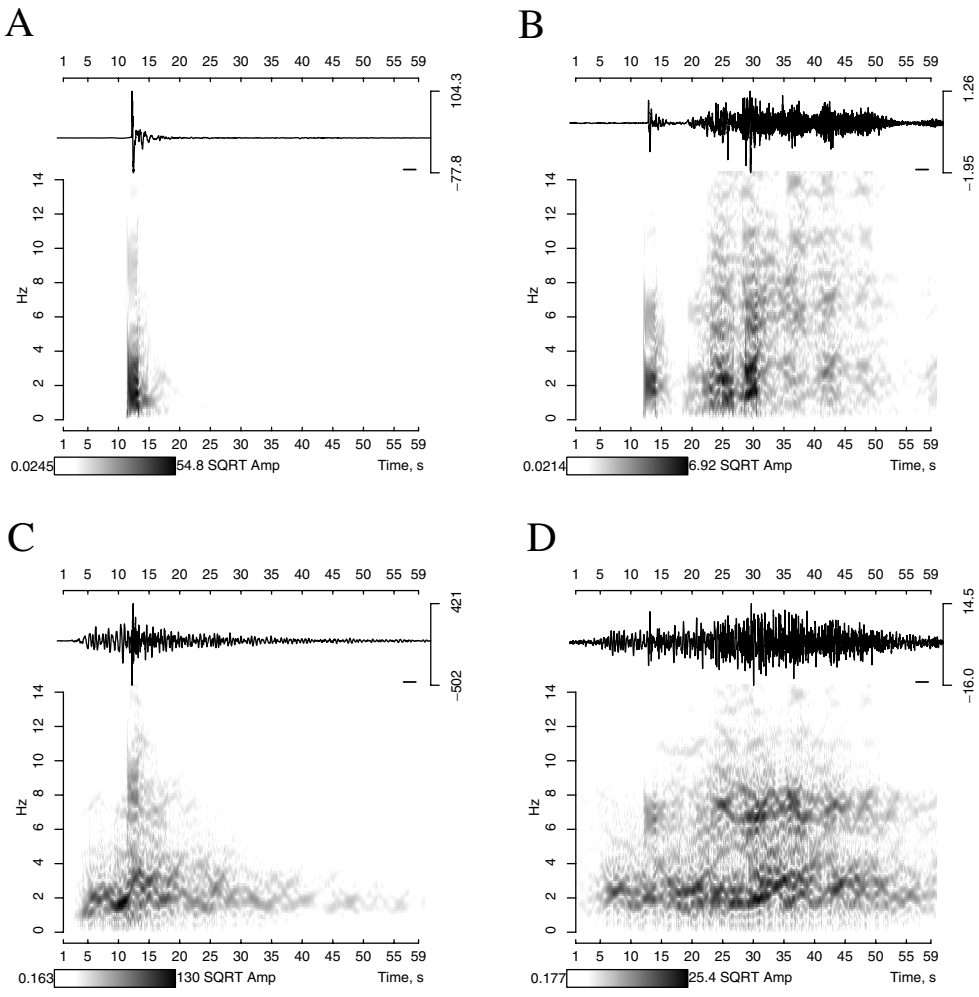

Fig. 4 Infrasound (**A–B**) and seismic (**C–D**) traces and spectrograms of explosions recorded at MAS station. Time scales are in seconds. Pressure amplitudes are in pascals and seismic amplitudes in μm/s. A *bar* over spectrograms shows the FFT window length (2 s). Left panels: Infrasound record of an EX event (07/21/2004 03h32) with a peak-to-peak pressure disturbance of 182 Pa. Onset is marked by a very clear arrival of a compression wave (A). Pressure decays exponentially with most of the pressure disturbance lasting about 4 s. Corresponding seismic record with a maximum ground motion peak-to-peak velocity is 923 μm/s. Ground-coupled infrasonic waves are recognized by their higher frequency content (C). Right panels: Infrasound record of an EX event with a large rumbling wave-train (08/4/2004 09h37 with a maximum pressure disturbance of 3 Pa) occurring after an impulsive onset (B). Corresponding seismic record with a maximum ground motion peak-to-peak velocity of 30 μm/s (D)

Chugging signals

In the course of this deployment, harmonic tremor 'chugging' (CH) events were recognized for the first time at Tungurahua. However, this does not mean that chugging signals were not produced in the past as acoustic monitoring at Tungurahua has been intermittent. Although relatively rare compared to other degassing signals, 16 events showed sequences of pulses at time intervals between 0.5 to 1.0 s (Fig. 5B and D), with a saw-tooth shape on infrasonic records, similar to chugging events observed on other active volcanoes (Hagerty et al. 2000; Johnson et al. 1998; Johnson and Lees 2000). Each pulse consists of an initial compression followed by a small rarefaction, resembling a periodic sequence of minor blast events. Seismic records of CHs have emergent onsets and tremor-like codas without clear distinctive pulses. Spectrograms of Tungurahua's CH events show that most of the energy is in the 1–3 Hz band and gliding (Garcés et al. 1998) is not apparent.

Clustering of explosive events

Quantitative cluster analysis was applied to the highest quality data in order to find populations of EX events with common characteristics. To extract a consistent data set, we used 361 events with reliable seismic and acoustic arrival-times at MAS (Fig. 2). Events with picking errors greater than 0.1 s were rejected. The high-quality events were partitioned using fuzzy logic R-software (Ihaka and Gentleman 1996; Kaufman and Rousseeuw 1990). A cross correlation matrix of all pairs of data is created and the dissimilarity matrix (D) is formed from the complement of the cross correlation. The matrix D is rotated by principal component analysis, such that the first component is the direction of maximum variance between dissimilarity coefficients, and the second component has maximum variance among all components perpendicular to the first (Pison et al. 1999). Clusters are graphically displayed on a principal component plot with ellipses containing all events of each cluster. Distance between ellipses measures the degree of dissimilarity between clusters. For a full description of the algorithm, see Pison et al. (1999).

Clusters of infrasonic signals

Prior to cluster analysis, signals were filtered using a band-pass 0.5–10.0 Hz Butterworth filter. Four second data windows with a 1-s pre-event window were considered

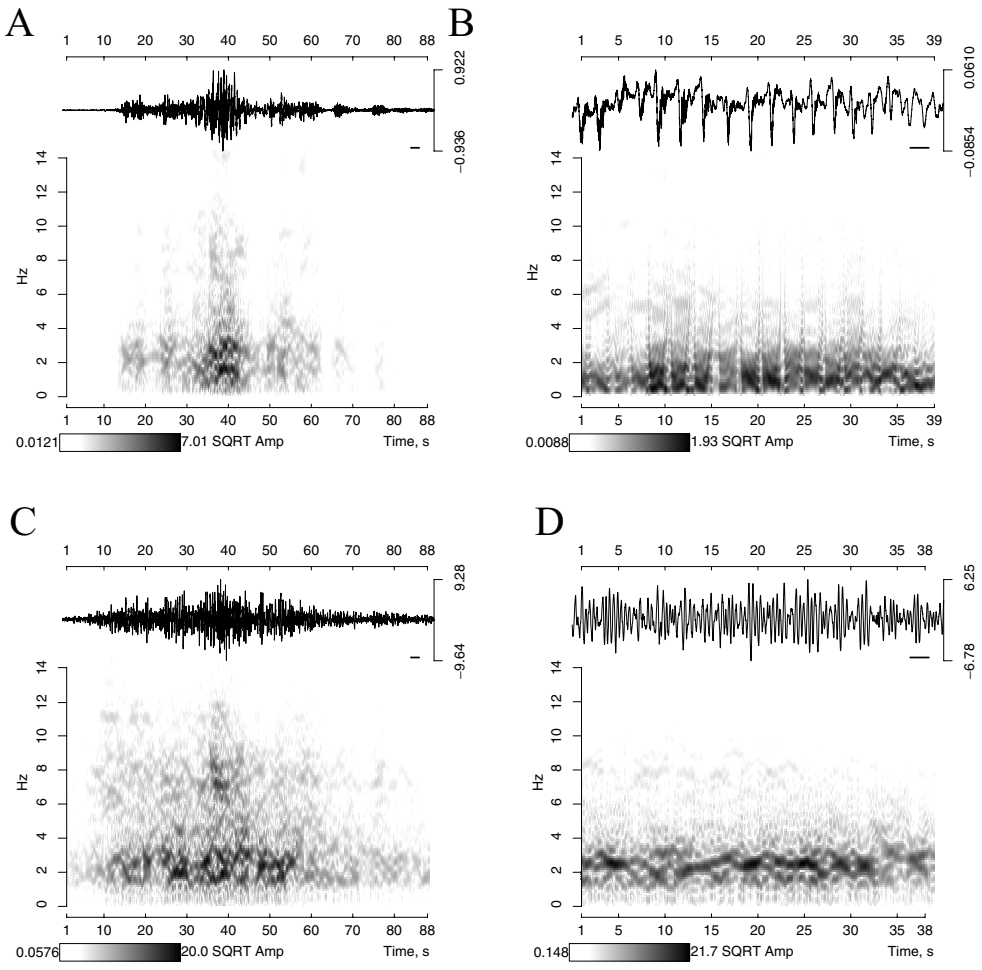

Fig. 5 Left panels: infrasound (**A**) and seismic (**C**) records of a jetting (RO) event (07/3/2004 04h50) at MAS station. Pressure amplitudes are in pascals and seismic amplitudes in μm/s. Infrasonic records show a chaotic wave-train with the largest amplitude of 2 Pa and most of the energy in the 1–10 Hz band. Seismic signals have a very emergent onset with the largest amplitudes of 19 μm/s. Right panels: CH event recorded at MAS station. **B** Infrasound record of an event on 07/3/2004 09h38, shows a sequence of pulses at regular time intervals starting at time 8 s, and becoming clear at time 22 s. Pressure disturbance of these events are generally small (0.17 Pa). **D** Corresponding seismic signals with a tremor-like appearance. Gliding is not clearly seen in Tungurahua's CH events. Note duration of CH and RO events. Time scales are in seconds. Infrasound amplitudes in pascals and seismic amplitudes in μm/s

for analysis. Cross-correlation scores for the full data set are generally low, so only high correlation pairs were selected for analysis. Cluster analysis was applied to a set of 28 events with correlation factors (σ) larger than 0.96. From this analysis, four distinct clusters were observed (Fig. 6). Using a hierarchical technique, a dendogram tree was produced for these events (Fig. 7). In this type of graph, adjacent events, represented as leaves, are the most similar. Clusters are grouped in branches with a length proportional to the level of dissimilarity ($1-\sigma$). Using such a method, the same four clusters of EX events were obtained. An inspection of stacked signals of these clusters shows the following characteristics:

- Group A1 (1, 9, 10, 17, 19, 23, 27) events (Fig. 8A) have a short duration compression phase (t_c=0.25 s), followed by long-duration rarefaction phase (t_r=0.43 s) with a large ratio between amplitudes of compression and rarefaction peaks, hereafter represented by ξ (ξ=0.962 for A1 cluster).
- Group A2 (2, 5, 8, 12, 13, 16, 20, 22, 24) events (Fig. 8B) have a very short compression time t_c=0.23 s, followed by a short duration rarefaction t_r=0.27 s. However, the compression /rarefaction ratio ξ=0.733 is small.
- Group A3 (3, 7, 14, 15, 21) events (Fig. 8C) have a short duration compression phase t_c=0.26 s, followed by a

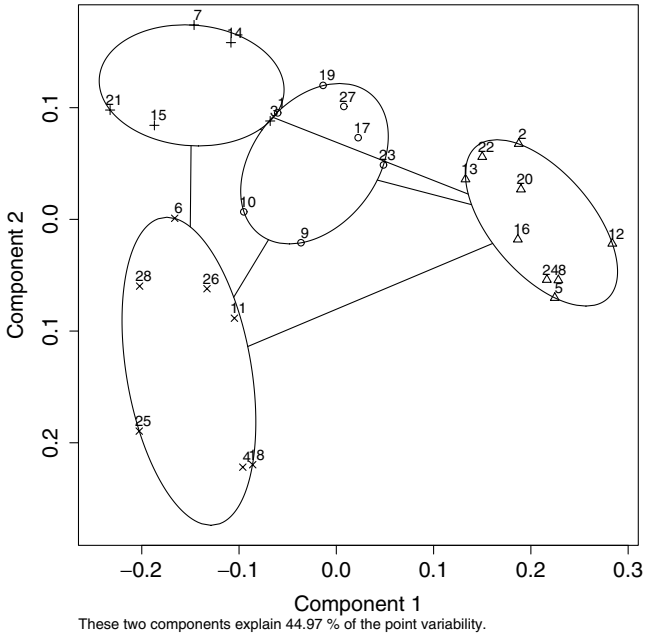

Fig. 6 Cluster distribution of infrasonic records after applying a fuzzy logic process. Four distinct clusters of EX events are *circled* and marked with distinct symbols (A1 *circle*; A2 *triangle*; A3 *vertical cross*; A4 *oblique cross*). Degree of dissimilarity between clusters is given by the length of *straight lines* connecting clusters

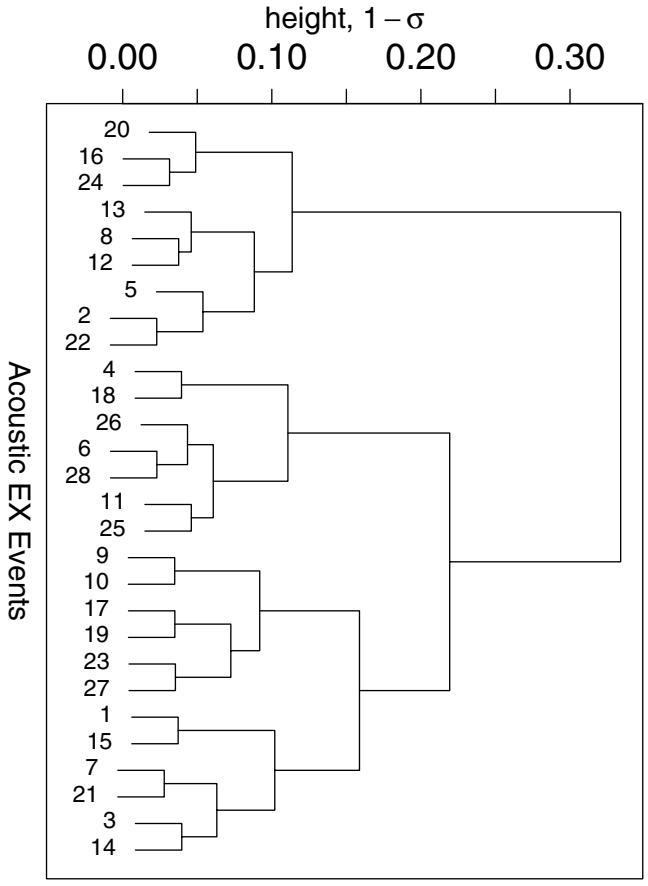

Fig. 7 Dendogram tree showing the event clustering of acoustic signals of explosion blast (EX) events. Length of the dendogram branches denotes the degree of dissimilarity between events or event groups between the data set. Also, four clusters of EX events were found by this method

very long-duration rarefaction phase t_r=0.51 s. Pressure ratio is high ξ=0.932, as in Group 1.

– Group A4 (4, 6, 11, 18, 25, 26, 28) events (Fig. 8D) have a low-frequency compression, and also low-frequency rarefaction (t_p=0.31 and t_r=0.49 s). Pressure ratio is small (ξ=0.667).

Other than the differences in waveform signature noted above, the infrasonic signal clusters show no other distinctive amplitude or temporal variations.

Clusters of seismic signals

Before performing a cluster analysis, we applied a band-pass filter (0.5–10.0 Hz) and integrated the corresponding seismic signals to seismic displacement. Initial arrivals of the seismic signals were selected with 4-s windows. The seismic signals are more complicated than the infrasonic signals due to path effects, and perhaps, source complexities. Clustering of the seismic signals was weaker than the acoustic signals. Only two poorly related groups (S1 and S2) were found using the same fuzzy logic process (Fig. 9). Stacked signals corresponding to seismic records of each cluster are presented in Fig. 10. Most of the events of acoustic group A1 (6 out of 7 events), and A2 (5 out of 7) belong to S1, and most of the events of A3 (8 out of 9 events) belong to S2. Events from cluster A4 are split between three events in S1 and two in S2. This apparent correlation between infrasonic and seismic clusters suggests that clusters are related to a source effect, due to the fact that these signals, traveling on completely different paths, show some degree of coherent clustering.

Table 3 Statistics of delay times between infrasonic and seismic arrivals of EX events

Station	*N* readings	Median (ΔT) (s)	$\Delta T_{5\%}$ (s)	$\Delta T_{95\%}$ (s)
MAS	361	10.062	9.359	12.602
JUI	24	11.904	10.998	16.175
RUN	164	16.854	16.293	18.943

Analysis of source locations

Delay times between impulsive pressure pulses and emergent seismic onsets ($\Delta T = T_{ac} - T_{p1}$), measured from 361 events with clear arrival times, were analyzed in order to constrain the explosion (EX) source locations. The distribution of these delays has a positive skew, with an apparent Poisson-type distribution (Fig. 11). Table 3 shows the median values and the 5th and 95th percentiles of ΔT. We found that the scatter in ΔT is not caused primarily by a atmospheric effect, because normal daily variations in ambient temperature were too small to produce the observed time anomalies. Average delay times between seismic and acoustic phases were analyzed for both night-time explosions and day-time explosions and show a difference of about 0.1 s for presumed cold and warm atmospheric conditions. This is significantly less than the observed scatter. Ambient winds could also affect acoustic arrival times. However consistent anomalies at all stations (azimuthal distribution of ~180 °), suggest that these delays are not caused by wind. Winds (0–5 m/s at 18,000 feet according to Instituto Geofisico, in unpublished weekly reports) were also too small to produce these anomalies. Thus, the large scatter of observed ΔT can be explained by these options: (1) a seismo-acoustic point source located at variable depth within the conduit, (2) a spatially-fixed point source with variable ascent velocity of erupted material, and (3) a spatially-extended source that has a varying source time function. In this paper, we address the first option in detail below and we discuss implications for the second option. Option (3) is beyond the scope of this paper because it requires detailed analysis of source time functions and mechanisms of the explosive volcanic events.

We assume that EX events originate as a point source at time T_o inside the conduit at a depth z below the crater floor with fixed elevation h_v~4,750 m. At this point, we consider that seismic waves are generated due to a gas expansion inside the conduit accompanied by a possible

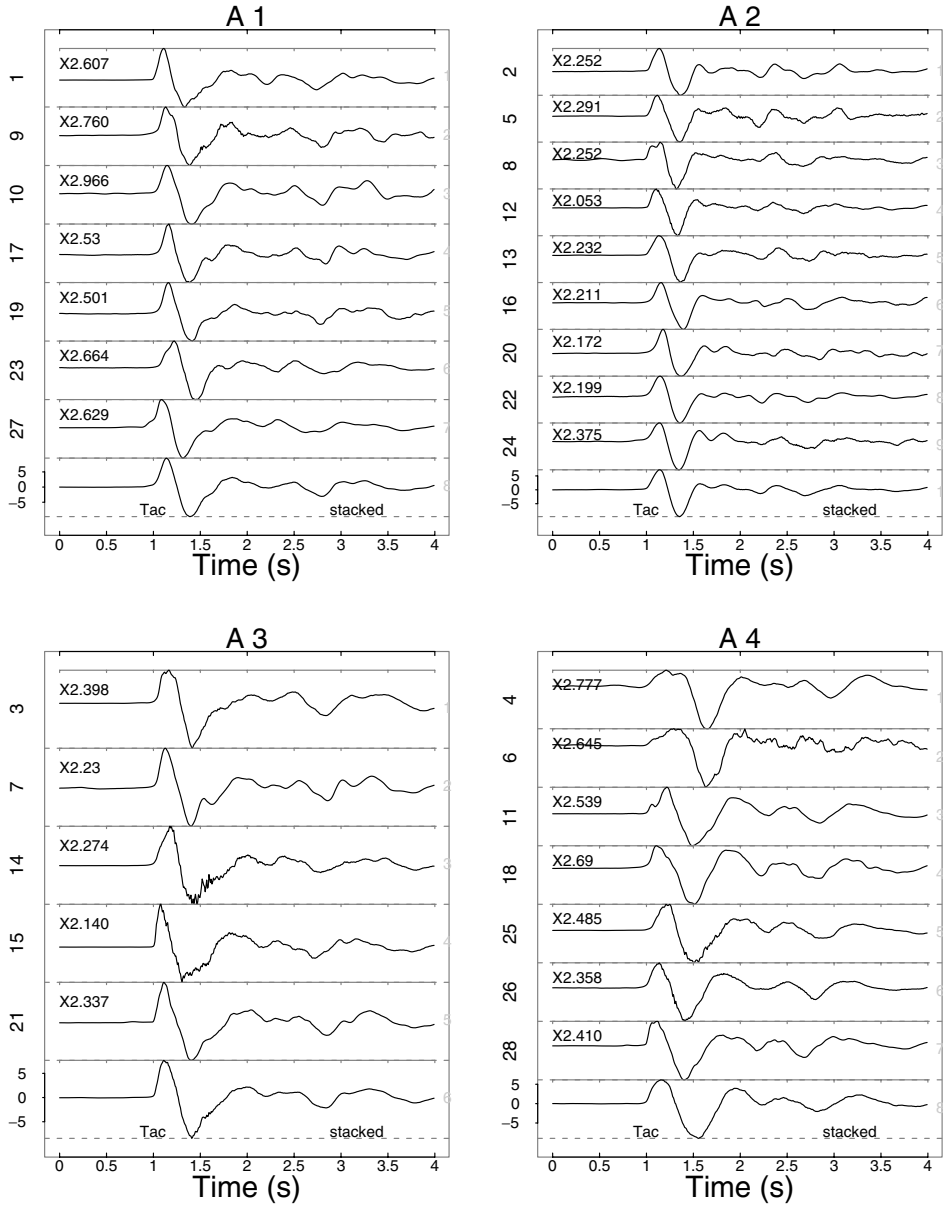

Fig. 8 Infrasonic records of each cluster of infrasound signals (*A1*, *A2*, *A3*, and *A4*). Last row is the stacked signal. Amplitudes of infrasound signals are normalized according to the stacked one (amplitude factor is given above each trace). Signals are aligned considering T_{ac} at time 1 s

brittle fracture. The initiation of the EX event thus corresponds to the onset of gas and ash rising through a narrow conduit (or system of cracks) towards the vent. For the sake of a simplistic model, we fix the rise velocity (U) of this two-phase fluid between the original source depth and the vent. Gas reaches the flaring portion of the conduit (i.e., the vent) near the crater floor at time (T_0+z/U), where it freely expands into the atmosphere and produces infrasound. Sudden volumetric expansion at the vent may also generate a secondary seismic pulse. These acoustic and secondary seismic waves propagate from the vent and arrive at the stations at times T_{ac} and T_{p2}, respectively (Fig. 12). The initial seismic pulse, corresponding to the event onset, arrives at time (T_{p1}=T_0+t_{pi}) at the station i (elevation h_i). For a temperature of 10°C, we calculate a corresponding air sound speed of v_{air}=337.6 m/s using Eq. (1.2) of Ford (1970). The following equations are used to estimate the travel times of first seismic and infrasonic waves:

$$t_{pi} = \frac{1}{\alpha}\left(\sqrt{d_{hi}^2 + (h_v - h_i - z)^2}\right) \tag{1}$$

$$t_{aci} = \frac{\sqrt{d_{hi}^2 + (h_v - h_i)^2}}{v_{air}} \tag{2}$$

And the time difference between arrivals is the following:

$$\Delta T_i = \frac{z}{U} + t_{aci} - t_{pi} \tag{3}$$

Where t_{pi} is the travel time of the first seismic pulse from the source to the station i, and, t_{aci} is the travel time of

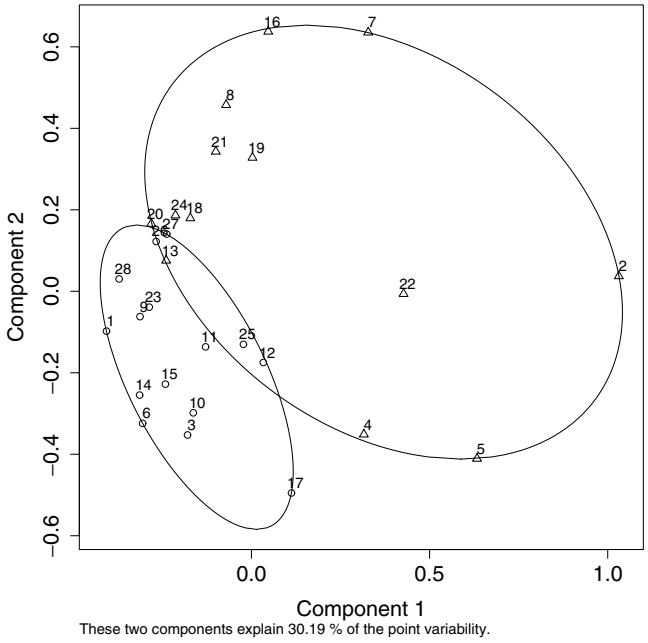

Fig. 9 Cluster distribution of corresponding seismic records after applying a fuzzy logic process. Two poorly constrained clusters: S1 (*circle*) and S2 (*triangle*) of explosion events are *circled*

acoustic wave from the crater to the station i (MAS, JUI or RUN). The horizontal distance from the conduit to the station i is d_{hi}, and α is the seismic velocity of the volcano edifice.

Using a seismic velocity of 2.9 km/s found by Molina (2001) for a half space velocity model for p waves at Tungurahua, variations in U and z, were investigated by minimizing the residuals between observed and predicted delay times (ΔT) at three stations (Eq. (3), Fig. 13). Minimum residuals show a clear trade-off between U and source depth (z): ($z = 0.925$, $U - 4.419$) in the ranges of U (10–300 m/s) and z (15–275 m).

The ascent rate of a two-phase fluid through a conduit or system of cracks is a very complex problem, which depends upon flow properties (density, viscosity) and path geometry (width, length, and wall roughness) (Papale 1998; Garcés 2000). At the vent, the gas-and-ash mixture is able to accelerate as it leaves the confines of the conduit (Nishimura and Chouet 2003; Johnson 2003). Owing to conservation of material flux, the conduit velocity (U) is assumed to be less than the initial ejection velocity at the vent (v_{ej}). Therefore, we calculated v_{ej} using the total acoustic power (Π) radiated by these events, based on the assumption that blast-type eruptions can be represented as an ideal monopole acoustic source (Woulff and McGetchin 1976). Total acoustic power, emitted during a time interval (T_{b}) in a half sphere of radius equal to the distance between the vent and the microphone, is easily calculated by integrating the square of pressure disturbance (Δp), using the following expression given by Vergniolle and Caplan-Aubech (2004):

$$\Pi = \frac{\pi r^2}{\rho_{\mathrm{air}} v_{\mathrm{air}} T_b} \int_0^{Tb} \Delta p^2 \mathrm{d}t \tag{4}$$

Gas exit velocities at volcanic explosions can be obtained using the expression given below (Woulff and McGetchin 1976):

$$v_{\mathrm{ej}} = \left(\frac{v_{\mathrm{air}} \Pi}{4\pi \mathrm{K_m} \rho_{\mathrm{air}} R_b^2} \right)^{1/4} \tag{5}$$

Constant $\mathrm{K_m}$=1/16 for monopole sources is given by Vergniolle and Caplan-Aubech (2004). Radius of the orifice

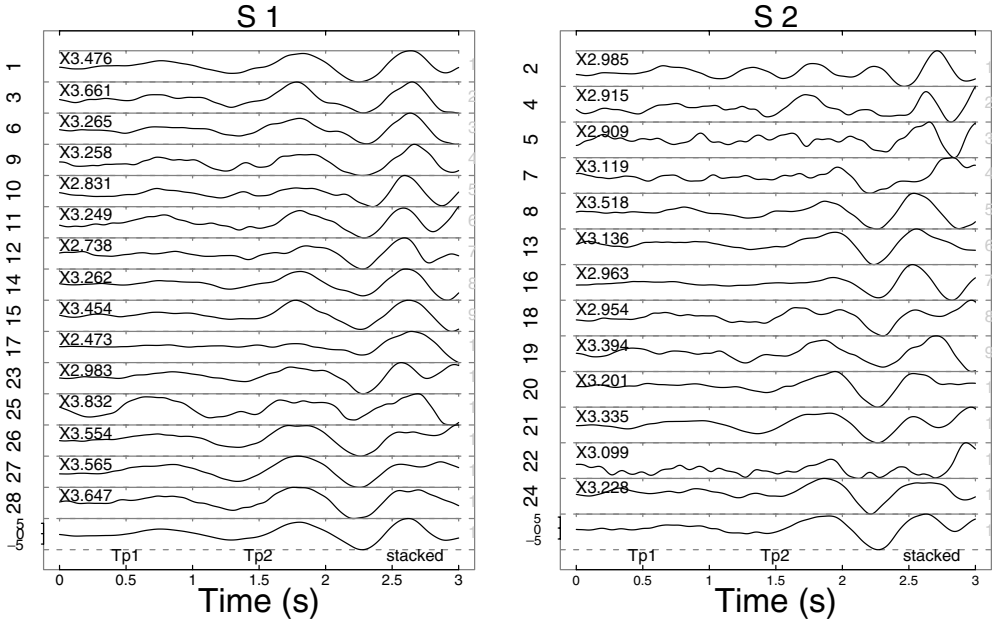

Fig. 10 Seismic records of S1 and S2 clusters. Last row is the stacked signal. Signals are aligned using cross-correlation lags with the first event. Traces have smooth arrivals of the first compression arrival (T_{p1}), however, stacked signal shows a clear arrival of T_{p2} phase. Amplitudes of infrasound signals are normalized with respect to the stacked one

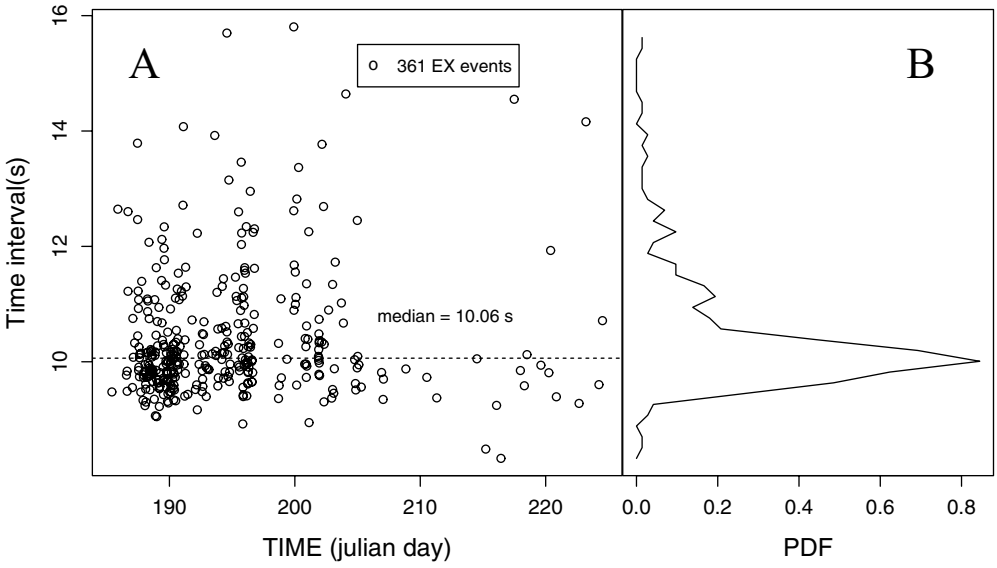

Fig. 11 **A** Time intervals between arrivals of acoustic pulse and first P-wave motion (ΔT) observed on MAS station at 3,516 m (total distance) from the vent. Notice the important spread that occurred even on the same date, showing that there is no time migration of explosion source and suggesting the presence of multiple sources. **B** Distribution of ΔT times shows a poisson-like distribution

R_b=10 m is estimated from oblique FLIR pictures taken by P. Ramón and F. Bocker in March 2003 (Samaniego et al., 2003), and air density (ρ_{air}) equal to 0.9 kg/m^3 (Batchelor, 1967). With Eq. (5), we found the gas ejection velocity for 361 explosion events of Tungurahua, with a median of v_{ej}=20 m/s and a maximum of 130 m/s. The median of v_{ej} represents a first order approximation for U. Gas ejection velocities v_{ej} reported on Strombolian explosions are in the range of (20–112) m/s (Chouet et al. 1974; Weill et al. 1992; Ripepe et al. 2001, 2002). For vulcanian explosions at Soufriere Hills, jet velocities varying from 40 to 140 m/s were measured (Formenti et al. 2003).

Once U and α are fixed, we used Eq. (3) to find the best fit source depth (z) in the conduit for EX events based on time differences between acoustic and seismic arrivals.

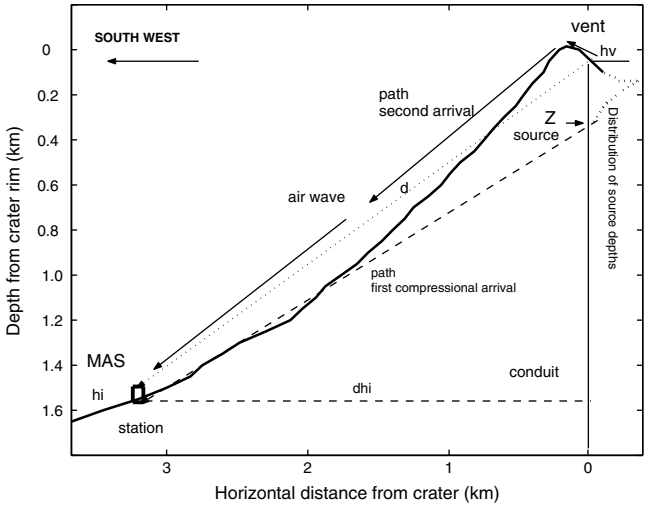

Fig. 12 Schematic propagation model for EX type events in Tungurahua volcano. Source is located at depth z below crater. From z, gas-and-solid material ascends at velocity U through the conduit, reaching the crater floor (altitude h_v) at time T_o+U/z. Secondary seismic and infrasound signals travel in almost parallel paths from the vent to the station at altitude h_i and horizontal distance to vent d_{hi}

Assuming a constant U, large variation of ΔT also implies a variation in source locations. Statistical estimates of z are given in Table 4 and Fig. 14. Considering the 5th and 95th percentiles of z, we found that the source of explosion events at Tungurahua extends from the crater floor down to ~100 m below. Although amplitudes of infrasonic clusters are not significantly different, clusters A1 and A2 have different depths at 10% significance. The shallow source depths of EX events are comparable to depth estimations of explosions on other volcanoes such as Arenal (Alvarado and Barquero 1987; Hagerty et al. 2000), Stromboli (Chouet et al. 1997, 2003; Ripepe et al. 2001), and Etna (Gresta et al. 2004), where depths of explosion sources are shallower than 260 m.

Using a higher ascending velocity (U=100 m/s), as might be expected for large explosions, we estimate an explosion depth range of ~50–200 m below crater. For U<20 m/s, z values are smaller than those reported on Table 4.

Stacked records of seismic explosion signals (Fig. 10) show the secondary compression phase (T_{p2}) arriving 1.0 s after the onset of the first seismic wave (T_{p1}). We assume that infrasonic wave and the secondary seismic pulse are both generated at the vent; and that both waves have nearly coincident ray-paths. Using the difference between these two arrival times, we can estimate α with a known propagation distance (d) and estimated sound speed as follows:

$$T_{ac} - T_{p2} = \left(\frac{1}{v_{air}} - \frac{1}{\alpha}\right) d \qquad (6)$$

Table 4 Statistical estimates of explosion source depth z

Station/ depth (z)	$z_{5th\ perc.}$ (m)	$z_{25th\ perc.}$ (m)	$z_{50th\ perc.}$ (m)	$z_{75th\ perc.}$ (m)	$z_{95th\ perc.}$ (m)
MAS	3	11	17	30	68
JUI	2	17	20	35	105
RUN	17	24	29	39	70

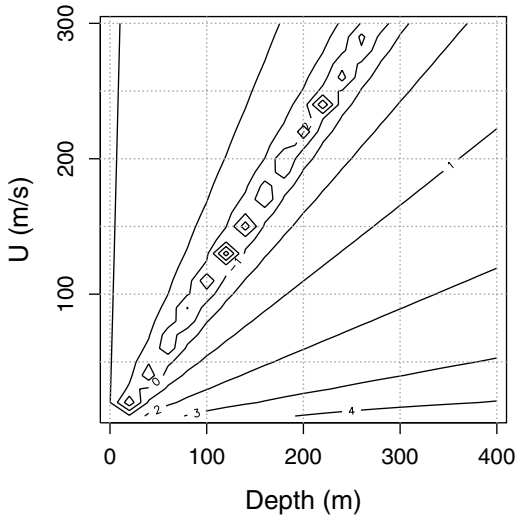

Fig. 13 Distribution of residuals between the observed delay times and the expected times of six EX events recorded at all stations, assuming a seismic source located in the conduit at depths between 0 to 400 m, for a range of U (10–300 m/s). *Contour lines* show that small residuals (in log scale) exhibit a linear trade-off between U and z

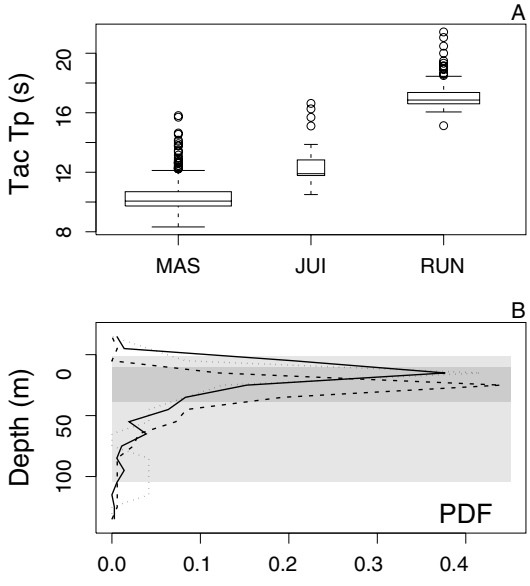

Fig. 14 **A** Observed ΔT delay times at MAS, JUI, and RUN. **B** EX source depths estimated using a model with a vertical conduit. The median value is indicated by a *line* inside the box. The *ends* of the box correspond to statistics called "hinges", which are similar to quartiles. Whiskers extend to values 1.5 times the inter-quartile range. Box widths are proportional to the square root of the number of elements in each data set

We note that observed delay times between the infrasonic and the secondary seismic phase match with a value of α=2.9 km/s, used in previous calculations.

Conclusions

During our seismo-acoustic deployment in 2004, Tungurahua volcano exhibited a diversity of degassing styles, characterized by single explosion blasts, long-duration jetting signals, and chugging signals. As compared to seismic records, infrasonic signals are considerably simpler, and thus provide a means for signal classification of explosion events. Four distinct cluster groups were recognized among the highly correlated explosion events. The groupings are based entirely on waveform similarity, and do not show any particular temporal pattern. Although at 10% significance, two infrasonic clusters have different source depths.

Large differences in arrival times of acoustic and seismic waves observed at Tungurahua, support a model where explosions occur at different depths inside the shallow part of the conduit (depth <200 m below the crater floor). Explosions start with a first pulse of seismic waves that exhibit a compressive polarity at all azimuths. After the event initiation, a two-phase mixture rises up through the conduit and arrives at the crater floor about 1 s later. Rapid gas expansion at the vent generates infrasonic compression waves and a secondary seismic pulse.

Acknowledgments Work presented in this paper was supported by NSF Grant EAR 0337462 and grant NSF EAR #0440225. We are thankful for the invaluable support provided by the Director and personnel of Instituto Geofisico, Ecuador and Tungurahua Volcano Observatory. We are also thankful to the field assistance of P. Ramón, D. Andrade, G. Ruiz, D. Barba, and N. Terán. M. Garcés and E. Marchetti along with their comments and suggestions for improving this work. We are grateful for the advice and technical support from the IRIS-PASSCAL instrumentation facility.

References

Alvarado G, Barquero R (1987) Seismic signals of Arenal volcano (Costa Rica) and their relationship with eruptive phases (1968–1986) (in Spanish). Ciencia y Tecnología, San Jose, Costa Rica 11:15–38

Batchelor GK (1967) An introduction to fluid dynamics, Cambridge University Press, Cambridge, pp. 1–615

Chouet BA, Hamisevicz NT, McGetchin TR (1974) Photoballistics of volcanic jet activity at Stromboli, Italy. J Geohys Res 79:4961–4976

Chouet BA, Saccorotti G, Martini M, Dawson P, De Luca G, Milana G, Scarpa R (1997) Source and path effect in the wavefield of tremor and explosions at Stromboli Volcano, Italy. J Geophys Res 102:15129–15150

Chouet BA, Dawson P, Ohminato T, Martini M, Saccorotti G, Giudicepietro F, De Luca G, Milana G, Scarpa R (2003) Source mechanism of explosions at Stromboli determined from Moment Tensor Inversions of very-long-period data. J Geophys Res 108 B1 2019, doi: 10.1029/2002JB001919

Egred J (2004) Eruptive History of Tungurahua volcano (in Spanish). Escuela Politécnica Nacional, Instituto Geofísico, in http://www.igepn.edu.ec/vulcanologia/tungurahua/historia.htm

Ford RD (1970) Introduction to acoustics, Elsevier, New York, pp. 1–149

Formenti Y, Druitt TH, Kelfoun K (2003) Characterization of the 1997 vulcanian explosions of Soufriere Hills Volcano, Monserrate, by video analysis. Bull Volcanol 65:587–605

Garcés M (2000) Theory of acoustic propagation in a multi-phase stratified liquid flowing within an elastic-walled conduit of varying cross-sectional area. J Volcanol Geotherm Res 101:1–17

Garcés MA, Hagerty MT, Schwartz SY (1998) Magma acoustics and time-varying melt properties at Arenal Volcano, Costa Rica. Geophys Res Lett 25:2293–2296

Garcés M, Iguchi M, Ishihara K, Morrissey M, Sudo Y, Tsutsui T (1999) Infrasound precursors to a Vulcanian eruption at Sakurajima Volcano, Japan. Geophys Res Lett 26:2537–2540

Gresta S, Ripepe M, Marchetti E, D'Amico S, Coltelli M, Harris AJL, Privitera E (2004) Seismoacoustic measurements during the July–August 2001 eruption of Mt. Etna volcano, Italy. Volcanol Geotherm Res 137:219–230

Hagerty M, Schwartz S, Garces M, Protti M (2000) Analysis of seismic and acoustic observations at Arenal Volcano, Costa Rica, 1995–1997. Volcanol Geotherm Res 101:27–65

Hall ML, Robin C, Beate B, Mothes P, Monzier M (1999) Tungurahua Volcano, Ecuador; structure, eruptive history and hazards. J Volcanol Geotherm Res 101:27–65

Ihaka R, Gentleman R (1996) R: a language for data analysis and graphics. J Comput Graphic Statist 5:299–314

Instituto Geofisico (2001) Annual Report of Tungurahua volcano activity: 2000 (in Spanish). http://www.igepn.edu.ec/vulcanologia/tungurahua/actividad/IAT2000.pdf

Instituto Geofisico-OVT (2004) Monthly summary of Tungurahua volcano activity: July 2004 (in Spanish). Escuela Politécnica Nacional, Departamento de Geofísica. http://www.igepn.edu.ec/vulcanologia/tungurahua/actividad/2004/2004-07.pdf

Johnson J (2003) Generation and propagation of infrasonic airwaves from volcanic explosions. J Volcanol Geotherm Res 121:1–14

Johnson JB, Lees JM, Gordeev EI (1998) Degassing explosions at Karymsky Volcano, Kamchatka. Geophys Res Lett 25:3999–4002

Johnson J, Lees JM (2000) Plugs and chugs: seismic and acoustic observations of degassing explosions at Karymsky, Russia and Sangay, Ecuador. J Volcanol Geotherm Res 101:67–82

Johnson J, Aster RC, Ruiz MC, Malone SD, McChesney PJ, Lees JM, Kyle PR (2003) Interpretation and utility of infrasonic records from erupting volcanoes. J Volcanol Geotherm Res 121:15–63

Johnson JB, Aster RC, Kyle RP (2004) Volcanic eruptions observed with infrasound. Geophys Res Lett 31:L14604, doi 10.1029/2004GL020020

Kaufman L, Rousseeuw PJ (1990) Finding groups in data: an introduction to cluster analysis. Wiley, New York, pp. 1–342

Molina I (2001) Pre-eruptive activity of Tungurahua volcano (in Spanish). Universidad de Caldas, Manizales, Colombia, pp 1–201

Nishimura T, Chouet B (2003) A numerical simulation of magma motion, crustal deformation, and seismic radiation associated with volcanic eruptions. Geophys J Int 153:699–718

Papale P (1998) Volcanic conduit dynamics in Freundt A., Rosi M., from magma to tephra. Elsevier, pp. 55–89

Pison G, Struyf A, Rousseeuw PJ (1999) Displaying a clustering with CLUSPLOT. ComputStatist Data Anal 30:381–192

Power JA, Lahr JC, Page RA, Chouet BA, Stephens CD, Harlow DH, Murray TL, Davies JN (1994) Seismic evolution of the 1989-90 eruption sequence of Redoubt volcano, Alaska. J Volcanol Geotherm Res 62:69–94

Ripepe M, Ciliberto S, Della Schiava M (2001) Time constraints for modeling source dynamics of volcanic explosions at Stromboli. J Geophys Res 106:8713–8722

Ripepe M, Harris A, Carniel R (2002) Thermal, seismic and infrasonic evidences of variable degassing rates at Stromboli volcano. J Volcanol Geotherm Res 118:285–297

Ruiz M, Hall M, Samaniego P, Ruiz G, Villagomez D (1999) Seismic activity in Tungurahua volcano: correlation between tremor and precipitation rates. Mem. 4th International Symposium on Andean Geodynamics, October 2005, Gottingen, Germany, pp 636–639

Ruiz M, Barba D, Johnson J, Seidl D (2001) Seismo-acoustic signals from Tungurahua volcano (in Spanish). Mem VI Jornadas Ciencias de la Tierra, EPN, Quito, Ecuador, pp 81–83

Samaniego P, Eissen JP, Le Pennec JL, Hall ML, Monzier M, Mothes P, Ramon P, Robin C, Egred J, Molina I, Yepes H (2003) Volcanic hazards related to Tungurahua (in Spanish), Corporacion Editora Nacional, Quito, Ecuador, pp 1–100

Tobin GA, Whiteford LM (2002) Community resilience and volcano hazard: the eruption of tungurahua and evacuation of the Faldas in Ecuador. Disasters 26:28–48

Vergniolle S, Caplan-Aubech J (2004) Acoustic measurements of the 1999 basaltic eruption of Shishaldin volcano, Alaska: 2. Precursor to the Sub-plinian phase. J Volcanol Geotherm Res 137:109–134

Weill A, Brandeis G, Vergniolle S, Baudin F, Bilbille J, Fevre JF, Piron B, Hill X (1992) Acoustic sounder measurements of the vertical velocity of volcanic jets at Stromboli volcano. Geophys Res Lett 19:2357–2360

Woulff G, McGetchin TR (1976) Acoustic noise from volcanoes: theory and experiment. Geophys J R Astr Soc 45:601–616